Dual wavelength operation of the GaSb-based Y-branch DBR lasers near 2.1 µm

J Jiang[1], L Shterengas[1], T Hosoda[1], A Stein[2], A Belyanin[3], G Kipshidze[2] and G. Belenky[1]

[1] State University of New York at Stony Brook, Electrical and Computer Engineering, Stony Brook, NY 11794, USA
[2] Brookhaven National Laboratory, Upton, NY 11973, USA
[3] Texas A&M University, College Station, TX 77843, USA

E-mail: leon.shterengas@stonybrook.edu

Received xxxxxx
Accepted for publication xxxxxx
Published xxxxxx

Abstract

The GaSb-based diode lasers operating simultaneously at two wavelengths near 2.1 µm have been designed and fabricated. The Y-branch devices used the 6th order distributed Bragg reflectors to provide spectrally selective feedback. The laser active region contained two asymmetric quantum wells with allowed optical transitions between two lowest electron (e1 and e2) and top hole (hh1) subbands. The laser emission lines loosely matched the e1-hh1 and e2-hh1 optical transitions with separation corresponding to ~3.1 THz. The 10-µm-wide deeply etched straight ridge DBR lasers demonstrated stable single mode operation with more than 50mW of output power.

Keywords: laser, GaSb, asymmetric quantum well, DBR, dual wavelength, Y-branch

1. Introduction

Dual-wavelength emission from monolithic semiconductor lasers is required for various applications including shifted excitation Raman difference spectroscopy (SERDS) [1], and intra-cavity difference frequency generation (IC-DFG) of THz radiation [2]. The devices for SERDS often operate in near-infrared region of spectra and utilize Y-branch design with two different distributed Bragg reflectors (DBR) serving as spectrally selective mirrors. The typical separation between two laser wavelengths is of the order of 30 cm^{-1}. The devices designed for difference frequency generation of ~3 THz require wider separation of the laser lines of the order of 100 cm^{-1}. The quantum cascade lasers (QCL) optimized for IC-DFG often rely on straight ridge designs incorporating two distributed feedback sections of different periods. The gratings in the QCLs are buried to facilitate heat removal and minimize the waveguide loss [3,4]. In case of the Y-branch DBR lasers for SERDS, no regrowth was used and the gratings had to be etched all the way through the top cladding layer of the complete laser heterostructure. The required high aspect ratio of the etching profile initiated development of the high order Bragg reflectors [5]. The use of Y-branch DBR interband lasers for IC-DFG can offer advantages over QCL technology in terms of threshold electrical power and ease of fabrication. The design of the interband active region with theoretically predicted resonant second order non-linearity was discussed in [6]. In this work we discuss the dual wavelength operation of the devices based on that active region. The demonstration of the dual wavelength operation of the GaSb-based lasers based on gain region with built-in resonant second-order nonlinearity is an important step towards development of the non-QCL low-threshold IC-DFG of THz radiation.

We report on design and development of the Y-branch 6th order DBR GaSb-based diode lasers emitting at 2.078 and 2.123 µm simultaneously. The dual-wavelength lasers utilized tunnel-coupled asymmetric quantum wells (QW) with

theoretically predicted strong resonant second-order nonlinearity [6]. The operating wavelengths of devices were loosely aligned to the mid-infrared optical transition energies of the three-level gain media of the asymmetric QWs. Note that in this integrated design there should be gain at both interband optical transitions involved in intracavity DFG, as opposed to any passive nonlinear interband QW devices in which external pumps would be absorbed at resonant transitions.

2. Heterostructure design and device fabrication

The diode laser heterostructure was grown on tellurium doped GaSb substrate by solid-source molecular beam epitaxy. Its active region contained two asymmetric QWs spaced by 20 nm waveguide core material. The active region was separated from claddings by 200 nm of $Al_{20}Ga_{80}As_2Sb_{98}$ layers. The 1.5 µm p- and 2 µm n-claddings were made of $Al_{60}Ga_{40}As_5Sb_{95}$ alloys. The asymmetric tunnel-coupled QWs contained three layers: ~12 nm of $Ga_{75}In_{25}Sb$; ~2 nm of $Al_{20}Ga_{80}As_2Sb_{98}$, and ~8 nm of $Ga_{92}In_8As_7Sb_{93}$. The resonant second-order nonlinearity of these QWs and operation of the corresponding four QW lasers with broadened waveguide were discussed in [6]. The number of QWs in active region of the laser heterostructures used in this work was reduced 2 and waveguide structure was redesigned to minimize the laser threshold current density. The second-order nonlinear coefficient $\chi^{(2)}$ of the three-band gain system is proportional to the product of the three dipole matrix elements corresponding to the e1-hh1, e2-hh1 and e2-e1 optical transitions (Figure 1).

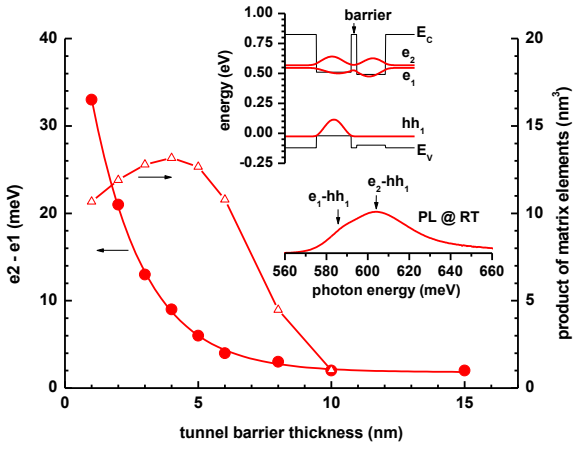

Fig. 1. The dependence of the energy splitting between two lowest electron states in the asymmetric QW on the thickness of the tunnel barrier. The right panel shows the corresponding dependence of the product of three dipole transition matrix elements. The insets show: top - the band diagram of the asymmetric tunnel-coupled QW and the electron and hole envelope functions; bottom – the experimental photo-luminescence spectrum of the laser wafer measured at room temperature.

Figure 1 shows the band diagram of the asymmetric QW together with calculated dependence of the splitting between e1 and e2 states and product of three matrix elements on the thickness of the tunnel barrier. The thickness of the tunnel barrier selected for this work led to splitting between e1 and e2 in the range of 15 - 20 meV as predicted by calculation and confirmed by experimental photoluminescence spectrum. The laser heterostructure described above was used to fabricate the deeply etched ridge waveguide lasers. The 100 and 10 µm wide Fabry-Perot devices were used as benchmarks. The 10 µm wide ridges were used for fabrication of the single mode DBR and dual wavelength Y-branch lasers.

Figure 2 illustrates the design and fabrication of the Y-branch DBR lasers. The straight ridge waveguides in branches were separated by 30 µm centre-to-centre. The Y-section merged the branches over the length of 1 mm ensuring smooth transition from two-ridge to one-ridge section. The one-ridge straight section was 1 mm long and its top metal had openings which were used to collect true spontaneous emission (TSE) spectra. The two-ridge straight section length was about 1.3 mm including ~600 µm long unpumped DBR in each branch. The total length of the Y-branch DBR devices was 3.3 mm. The reference straight ridge DBR lasers with grating periods of 1756 nm (DBR1756) and 1798 nm (DBR1798) were fabricated next to the Y-branch devices on the same wafer and had the same 3.3 mm length. The ridges were etched through the active region down to n-cladding layer (left inset in Figure 2) resulting into strong lateral current and optical confinements.

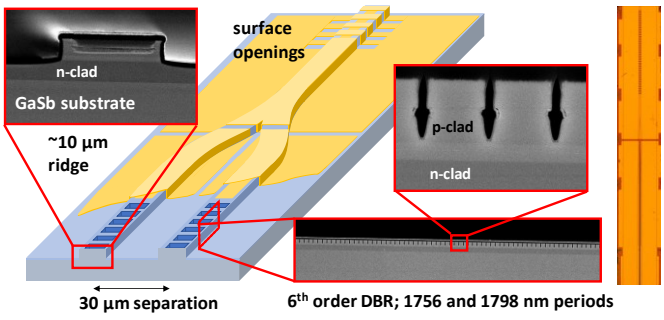

Fig. 2. The Y-branch laser with 1 mm one-ridge straight section, 1 mm Y section, 700 µm two-ridge straight sections, and 600 µm 6th order DBR sections with periods of 1756 and 1798 nm. The insets show the SEM images of the ridge and DBR etching profiles as well as optical image of the fabricated devices from top view (right).

The 6th order gratings were fabricated by chlorine-based inductively coupled plasma reactive ion etching. The gratings were etched down to the interface between p-cladding and waveguide core (right inset in Figure 2). The width of the high index sections (not etched) of the gratings was maximized to increase coupling to the laser mode [5]. The laser facets were

left uncoated and devices were soldered epi-side up onto gold-plated copper blocks for characterization.

3. Characterization results and discussion

The threshold current densities of the 100 µm wide uncoated Fabry-Perot lasers were about 110 and 70 A/cm^2 for 1-mm- and 3-mm-long devices, respectively (Figure 3a). These values are very close to threshold current densities reported previously for 2.2 µm high-power lasers based on active region with 2 standard symmetric QWs [7]. The injection efficiency and internal optical loss as estimated from variable-cavity-length analysis were about 80% and 5 cm^{-1}, respectively. Figure 3b shows the temperature dependences of the threshold current densities of the 100-µm-wide 3-mm-long and 10-µm-wide 3.1-mm-long deeply etched Fabry-Perot ridge lasers. The parameter T_0 of 100 µm devise was about 78 K in the temperature range from 20 to 60 ^{0}C.

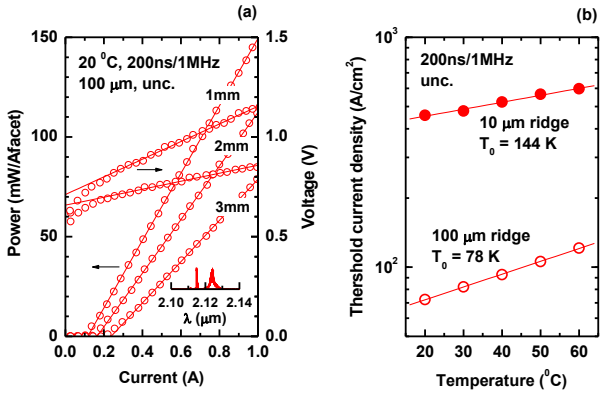

Fig. 3. (a) Power-current characteristics of the uncoated 1, 2 and 3 mm long 100 µm wide lasers measured at 20 ^{0}C in pulsed regime (200ns/1MHz). Voltage is shown for 1- and 3-mm long lasers. Inset shows the emission spectra near threshold for 1- and 3-mm long devices; (b) The dependence of threshold current density on temperature for 100-µm-wide 3-mm-long and 10-µm-wide 3.1-mm-long lasers.

The 10 µm wide lasers demonstrated about 6 times higher threshold current densities (Figure 3b) but only ~10% lower slope efficiencies (not shown) compared to 100 µm wide devices. The order of magnitude increase of the threshold current density in narrower ridges implies large surface recombination velocity (order of 10^6 cm/s) at the etched mesa side walls [8]. The intensive surface recombination strongly reduces effective carrier lifetime leading to dramatic increase of the threshold current density. However, the pinning of the QW concentration at the laser threshold minimizes the effect of the mesa side wall recombination leakage on laser efficiency. The twofold increase of the parameter T_0 in 10 µm devices (Figure 3b) compared to 100 µm ones supports this scenario. Indeed, when the laser threshold is controlled by short defect-like recombination lifetime the relative temperature sensitivity of the laser threshold current gets reduced. The threshold currents of the 10 µm wide ridge lasers will be decreased several times in the shallow ridge design without etching through the active region. However, the need for the precise control over the etching depth would eliminate the possibility to perform etching of the DBR gratings and ridge mesas simultaneously. The etching rate in narrow openings (~200 nm wide) of the grating hard mask is ~2 times slower compared to the etching in wide channels. Thus, two separate etching steps will be required to achieve adequate coupling of the laser mode to the grating and to minimize the device threshold.

The individual 10 µm wide DBR lasers with 2.7 mm long straight ridge section and 600 µm long DBR section demonstrated threshold currents of about 150 mA (Figure 4). The reference 10-µm-wide 3.1-mm-long Fabry-Perot devices showed similar threshold currents. As expected, the Fabry-Perot lasers emitted wide irregular spectrum with characteristic thermal red shift observed at increased currents. The DBR1798 devices with the DBR mirror providing selective feedback close to the gain peak generated narrow-spectrum output at 2.123 µm (~584 meV) with minimal thermal red shift. The DBR1798 lasers demonstrated monotonous increase of the output power with current. The strongly detuned DBR1756 lasers operated at DBR-stabilized wavelength of 2.078 µm (~597 meV) at currents only up to ~500 mA.

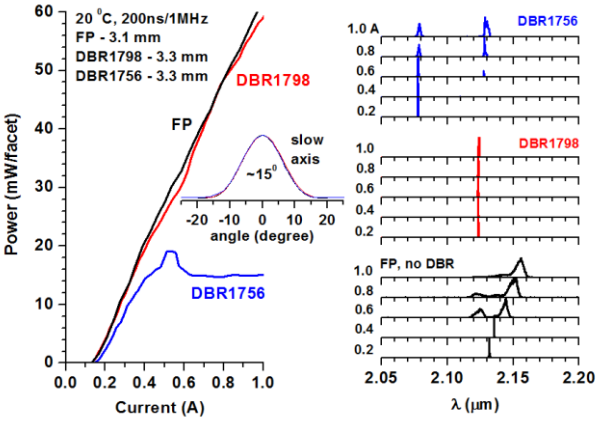

Fig. 4. Left: Power-current characteristics of the uncoated 10-µm wide 3.1 mm long Fabry-Perot and 3.3 mm long DBR lasers measured at 20 ^{0}C in pulsed regime (200ns/1MHz). The inset shows the calculated and measured (400 mA) lateral far field patterns of DBR lasers; Right: The laser emission spectra measured at several currents above threshold.

Both DBR lasers demonstrated stable single spatial mode operation characterized by current independent far field patterns. The slow-axis far filed divergence was ~15 degrees full-width-at-half-maximum (inset in Figure 4) which matched the calculation for the fundamental lateral mode. Notably, the deeply etched 10 µm wide ridges support more

than 20 lateral modes but we observed lasing only at the fundamental mode.

The effect of the DBR section length on the laser performance was studied experimentally using DBR1798 devices with minimal detuning. The DBR section provides not only necessary feedback in 6th order of diffraction but also introduced the radiation loss associated with lower orders. The radiation loss will increase the effective laser internal loss. Both the increased reflectivity of the DBR mirror and radiation loss will change the power levels emitted from cleaved and DBR facets. The calculated ratio of the front- and back- facet efficiencies as a function of the DBR mirror reflectivity is plotted in Figure 5. The calculation was performed for the device with front mirror comprising cleaved facet (~31% reflectivity) and back DBR mirror with varied reflectivity [9].

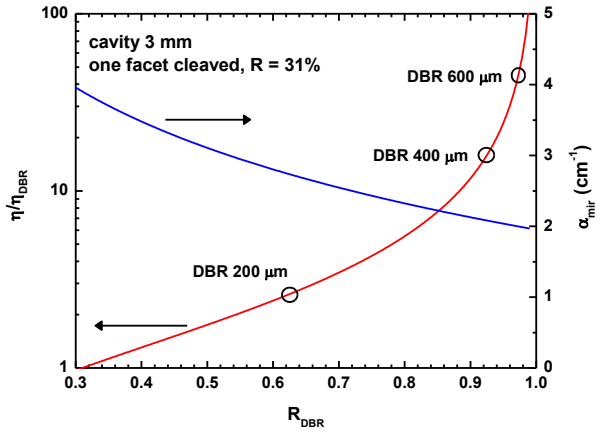

Fig. 5. The calculated dependence of the ratio of facet efficiencies of DBR laser versus DBR mirror reflectivity and the corresponding calculated distributed mirror loss for 3 mm long lasers. The open circles indicate the experimental values of the ratio of the facet efficiencies for devices with 200, 400 and 600 µm long DBR1798 sections.

We measured the power emitted from cleaved and DBR facets for DBR1798 devices with varied length of the DBR sections, namely, 200, 400 and 600 µm. The cavity lengths were 2.4, 3.1 and 3.3 mm, respectively. The comparison of the calculated and measured facet efficiencies allows estimating the reflectivity of the DBR mirrors of different lengths (Figure 5, open circles). The DBR length above 400 µm yields reflectivity in excess of 90% which corresponds to almost all laser power being emitted from the cleaved facet. The corresponding mirror loss becomes ~2 cm^{-1}, i.e. twice lower than in devices of the same cavity length with both facets cleaved. The facet slope efficiency of the uncoated Fabry-Perot device with mirror loss of about 4 cm^{-1} and total loss of about 9 cm^{-1} should be proportional to ~0.5*(4 cm^{-1} / 9 cm^{-1}), while that for DBR1798 laser to ~1*(2 cm^{-1} / 7 cm^{-1}) if the radiation loss were ignored. The same front facet efficiencies and threshold currents (see Figure 4) can be obtained if one assumes that 600 µm long DBR section introduced additional distributed optical loss of about 2 cm^{-1}.

The emission spectrum of the DBR1798 laser is single mode at 20 ^{0}C at any current (Figure 4). At currents above ~500 mA the emission spectrum of DBR1756 lasers became multimode with additional line appearing near the gain peak. Thermal red shift of the gain peak gradually increases DBR detuning and leads to multimode operation. The change of emission spectrum is accompanied by saturation of the output power level. Apparently, the gain at the wavelength corresponding to the e2-hh1 transition was inadequately low. In order to increase the gain at 2.078 µm one can reduced the device operating temperature. For demonstration of the dual wavelength operation of the Y-branch lasers we decreased the heatsink temperature down to 10 ^{0}C for pulsed regime and down to 2 ^{0}C for CW.

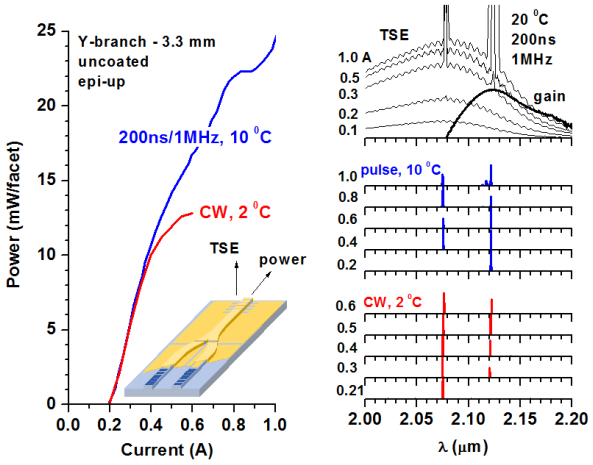

Fig. 6. Power-current characteristics of the Y-branch lasers measured at 10^{0}C in pulsed regime (200ns/1MHz) and at 2^{0}C in CW. Inset shows schematically how output and TSE spectra were measured. The right panel shows the TSE (top) and laser emission spectra (middle and bottom) of Y-branch lasers. The gain spectrum of the Fabry-Perot laser near threshold is plotted together with TSE spectra to illustrate the detuning of the 2.078 µm line at 20^{0}C.

Figure 6 shows the power-current characteristics and emission spectra of the Y-branch devices. After moderate cooling the gain peak shifted to shorter wavelength and lasers operated in dual wavelength regime. The CW output power in dual wavelength operation was above 10 mW. The TSE spectra collected at 20 ^{0}C are shown together with measured gain spectrum of the 1 mm long Fabry-Perot lasers. The gain peaks at wavelength corresponding to e1-hh1 transition. The lack of optical gain at e2-hh1 transition energy indicates inadequate transition matrix element value. The wavefunction overlap corresponding to e2-hh1 transition can be reduced under injection due to polarization of the asymmetric QW. This effect was not taken into account yet in the design of the

active region of the lasers discussed in this work. This explains the need to cool the Y-branch devices to achieve stable dual wavelength operation. The optical gain corresponding to the e2-hh1 transition must be increased in the IC-DFG lasers by either redesigning of the asymmetric QWs or adding extra QW to provide gain at shorter wavelength. The former is preferred approach since it would also improve the nonlinear conversion efficiency.

Figure 7 (centre, dots) shows the measured far field patterns of Y-branch devices at several currents above threshold. In contrast to individual DBR lasers (Figure 4) the Y-branch devices demonstrate apparent dependence of the beam shape on injection current. There is also a correlation between laser emission spectrum (Figure 7, right) and far field pattern.

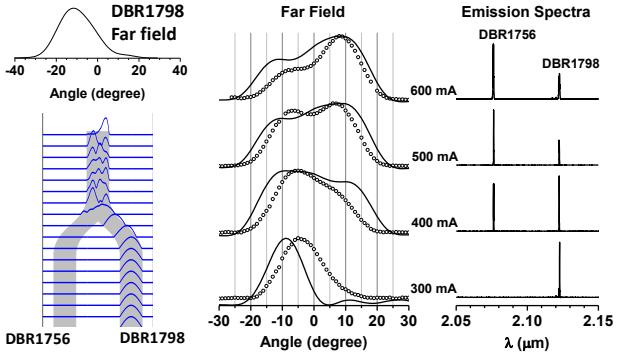

Fig. 7. Left: The simulated far field pattern and corresponding beam propagation profiles in Y-branch cavity with fundamental mode of the straight ridge launched in the right branch; Centre: The experimental (dots) and simulated (lines) far field patterns corresponding to different currents; Right: the Y-branch laser emission spectra at different currents.

The left panel of Figure 7 shows the simulated beam propagation in Y-branch cavity. The fundamental mode of the straight ridge waveguide was launched into the right branch (marked as DBR1798 to match the experimental device structure). As expected, the fundamental mode remains stable until it enters Y-branch section. In the Y-branch section it is not eigenstate and starts exciting higher order modes. The field propagating in the one-ridge straight section is already multimode. Depending on the phase, i.e. length of the one-ridge section, the multimode far field can be steered left or right from normal direction (see calculated far field in Figure 7, left, top). In experiment we observed that when laser emission spectrum contains the wavelength corresponding to DBR1798 branch of the two-ridge section, the far field is steered to the left (Figure 7, centre, dots, 300 mA). Once the current increases the line corresponding to DBR1756 appears in the laser emission spectrum. The far filed feature steered to the right becomes apparent (Figure 7, centre, dots, 400 and 500 mA). Once the DBR1756 spectral peak intensifies the far field pattern main peak moves to the right (Figure 7, centre, dots, 600 mA). This behaviour can be qualitatively reproduced in simulation (Figure 7, centre, lines) by changing relative intensities of the fundamental modes launched into the left and right branches.

4. Conclusion

The dual-wavelength operation of the GaSb-based Y-branch lasers with more than 20 mW of output power was demonstrated. The devices utilized 6th order DBRs to stabilize the emission spectrum at 2.078 and 2.123 μm wavelength, which corresponded to frequency difference near 3.1 THz. The laser active region contained two asymmetric tunnel-coupled QWs with allowed e1-hh1 and e2-hh1 transitions and built-in resonant second-order nonlinearity for generation of the e2-e1 difference frequency photons. The 10 μm wide deeply etched DBR lasers operated in spatially single mode regime confirming ability of the DBR to stabilize the modal structure of multimode waveguides. Intensive recombination at the etched mesa sidewalls led to nearly 6 times higher threshold current densities in 10 μm ridge lasers compared to 100 μm ones. The use of shallow ridge design will reduce the laser threshold current. The stability of the dual wavelength operation at elevated temperatures should be improved by increase of the optical gain at e2-hh1 transition. This can be achieved by modification of the asymmetric QW design to improve the oscillator strength of e2-hh1 transition under strong population inversion condition. Alternatively, the symmetric QW can be added to the laser active region to provide extra gain. The devices with improved spectral stability and minimized threshold current density can be applied to development of the new class of interband IC-DFG of THz radiation.

Acknowledgements

This work was funded by the National Science Foundation (NSF) through the grant ECCS-1707317US. This work was partially supported by the U.S. Department of Energy, Office of Basic Energy Sciences, through the Centre for Functional Nanomaterials, Brookhaven National Laboratory, under Contract DE-SC0012704.

References

[1] Sumpf B, Kabitzke J, Fricke J, Ressel P, Müller A, Maiwald M and Tränkle G 2016 *Opt. Lett.* **41** 3694-97

[2] Fujita K, Jung S, Jiang Y, Kim J H, Nakanishi A, Ito A, Hitaka M, Edamura T and Belkin M A 2018 *Nanophotonics* **7** 1795-817

[3] Evans A, Yu J, David J, Doris L, Mi K, Slivken S and Razeghi M 2004 *Appl. Phys. Lett.* **84** 314-16

[4] Troccoli M, Corzine S, Bour D, Zhu J, Assayag O, Diehl L, Lee B, Hofler G and Capasso F 2005 *IET Electron. Lett.* **41** 1059-60

[5] Fricke J, John W, Klehr A, Ressel P, Weixelbaum L, Wenzel H and Erbert G 2012 *Semicond. Sci. Technol.* **27** 055009

[6] Jiang J, Shterengas L, Hosoda T, Belyanin A, Kipshidze G and Belenky G 2018 *Appl. Phys. Lett.* **113** 071106
[7] Liang R, Chen J, Kipshidze G, Westerfeld D, Shterengas L and Belenky G 2011 *IEEE Photon. Technol. Lett.* **23** 603-05
[8] Coldren LA, Corzine SW, "Diode Lasers and Photonic Integrated Circuits", New York: Wiley, 1995
[9] Agrawal GP, Dutta NK, Agraval book, "Semiconductor Lasers", 2nd Ed, New York, Van Nostrand Reinhold, 1993